Neutron scattering investigation of magnetic phase transitions and crystal-field splitting in UX_3 (X identical to Br, Cl)

1990 J. Phys.: Condens. Matter 2 3369

(http://iopscience.iop.org/0953-8984/2/14/021)

J. Phys.: Condens. Matter **2** (1990) 3369–3380. Printed in the UK

Neutron scattering investigation of magnetic phase transitions and crystal-field splitting in UX_3 (X≡ Br, Cl)

B Schmid†§, A Murasik†‖, P Fischer†, A Furrer† and B Kanellakopulos‡

† Labor für Neutronenstreuung, Eidgenössische Technische Hochschule Zürich, 5232 Villigen PSI, Switzerland

‡ Institut für heisse Chemie, Kernforschungszentrum Karlsruhe, Federal Republic of Germany

Received 17 March 1989, in final form 27 November 1989

Abstract. Neutron scattering experiments were performed in the temperature range from 1.5 to 293 K on polycrystalline samples of the non-metallic $5f^3$ electron systems UBr_3 and UCl_3. The hexagonal crystal structure $P6_3/m$ was refined at $T = 293$ and 10 K. UBr_3 orders at $T_N = 5.4(1)$ K with a second-order transition to a 0+ − configuration of magnetic moments of magnitude $\mu_U^{(3.9K)} = 2.08(2)\mu_B$ oriented parallel to the c axis. At $T_t = 3.0(5)$ K occurs a second transition to an ordered antiferromagnetic ground state, corresponding to the lattice constants $a_m = \sqrt{3}a$, $b_m = a$, $c_m = 2a$. This structure is anticentered in the basal plane. The magnetic moments of magnitude $\mu_U^{(1.6K)} = 0.82(4)\mu_B$ are oriented parallel to the b axis. In both magnetic phases the antitranslation $(0, 0, \frac{1}{2})$ suggests predominantly antiferromagnetic exchange within the chains of uranium ions along the c axis. The situation is similar for UCl_3: the first transition at $T_N = 6.5(1)$ K with an ordered magnetic moment $\mu_U^{(4.0K)}$ of $1.8(1)\mu_B$, and the second transition at $T_t = 3.8(5)$ K with a magnetic moment $\mu_U^{(1.6K)}$ of $0.8(1)\mu_B$. By means of inelastic neutron scattering we have measured the crystal-field splitting of UBr_3 and UCl_3 and determined the crystal-field parameters. The assumption of anisotropic magnetic interactions reasonably predicts the value of the zero-field magnetisation and provides an explanation for the magnetic phase transitions.

1. Introduction

Trihalides UX_3 (X ≡ F, Cl, Br, I) of uranium are non-metallic $5f^3$-electron systems with a $^4I_{9/2}$ ground state of the U^{3+} ions. UF_3 crystallises with a hexagonal structure of the LaF_3 type (Berger and Sienko 1968, Brown 1968). Both UCl_3 and UBr_3 crystallise in the hexagonal UCl_3 structure type corresponding to space group $P6_3/m$ (Taylor and Wilson 1974, Levy *et al* 1975b, Murasik *et al* 1985). On the other hand, UI_3 has the orthorhombic $PuBr_3$ structure (Levy *et al* 1975a, Murasik *et al* 1981). Whereas bulk magnetic measurements performed on UX_3 show for UF_3 (Berger and Sienko 1968) no evidence of an antiferromagnetic transition down to 1.9 K, Néel temperatures of 22 K, 15 K and 3.4 K were reported (Jones *et al* 1974) for UCl_3, UBr_3 and UI_3, respectively,

§ Present address: Reactor Radiation Division, National Institute of Standards and Technology, Gaithersburg, MD 20899, USA.

‖ Permanent address: Institute of Atomic Energy, 05-400 Otwock Swierk, Poland.

0953-8984/90/143369 + 12 $03.50

based on the observed maxima of the magnetic susceptibilities. The cooperative magnetic phenomena in these systems depend on electronic factors associated with exchange interactions, crystal-field effects and spin–orbit coupling. Recently (Murasik *et al* 1985), the magnetic properties of UCl_3 were interpreted on the basis of uranium chains along the c axis with predominant antiferromagnetic intrachain and weaker interchain interactions. From inelastic neutron scattering experiments, evidence for the magnetically one-dimensional nature of the 5f compound UCl_3 was found. One-dimensional magnetism in the vicinity of the Néel temperatures derived from bulk magnetic measurements would explain the considerably lower Néel temperature in these systems determined by neutron diffraction.

In this paper we report on new neutron scattering results obtained for UBr_3 and UCl_3 which prove long-range antiferromagnetism with one disordered magnetic sublattice below $T_N = 5.4(1)$ K and 6.5(1) K, respectively and the occurrence of another magnetic phase transition with a reorientation of the magnetic moments at $T_t = 3.0(5)$ K and 3.8(5) K for UBr_3 and UCl_3, respectively. The new neutron spectroscopy data for UBr_3 and UCl_3 were successfully interpreted. On the basis of the crystal-field parameters derived from the spectroscopic data presented in this work we arrive at eigenfunctions which predict the observed zero-field magnetisation as well as the second-phase transition at T_t which is found to result from anisotropic magnetic interactions, combined with crystal-field effects. Both UCl_3 and UBr_3 show inelastic neutron scattering features of one-dimensional magnetism at higher temperatures.

2. Neutron diffraction analysis

Neutron diffraction experiments were performed with use of both the multidetector powder spectrometer and the two axis diffractometer at the reactor Saphir in Würenlingen. The measurements were carried out in the temperature range from 1.5 to 293 K on polycrystalline samples enclosed under a He gas atmosphere in cylindrical vanadium containers of 1 cm diameter and 5 cm height. UBr_3 and UCl_3 were prepared in Poland (cf Murasik *et al* 1986), and a new sample of UCl_3 originates from the Kernforschungszentrum Karlsruhe. The samples proved to be pure and stoichiometric.

For the structure analysis, nuclear neutron diffraction patterns with about 350 inequivalent contributing reflections were measured with a neutron wavelength λ of 1.186 Å (Ge 311 monochromator; no $\lambda/2$ contribution). A profile analysis of the data, including a minor correction for the preferred orientation [001] was made, using the program of Wiles and Young (1981) including a background fit (figure 1).

The results which are summarised in table 1 confirm the UCl_3-type structure for both compounds. Figure 2 shows the ninefold coordination of the uranium ions with selected interatomic distances for consideration of crystal-field and magnetic interactions. To separate the coherent magnetic intensity, difference diagrams were calculated and smoothed concerning spurious maxima and minima caused by slight shifts of large peaks. The 7.2 K diagrams were found to be identical with the 20 K patterns of UBr_3 and UCl_3. The essential sections of the magnetic low-temperature diagrams are shown for UBr_3 in figure 3. For 5 and 6 K, the magnetic Bragg reflections may be indexed on the basis of a hexagonal unit cell with lattice constants $a_m = \sqrt{3}a$, $c_m = 2c$ (wavevector $\boldsymbol{q}_0 = [\frac{1}{3}, \frac{1}{3}, \frac{1}{2}]$) which corresponds to three magnetic sublattices. The absence of magnetic peaks with $h = 3n$, where n is an integer (using the magnetic unit cell with $a_m = 3a$; see figure 3 referring to the chemical cell) indicates a zero vector sum of the magnetic moments of

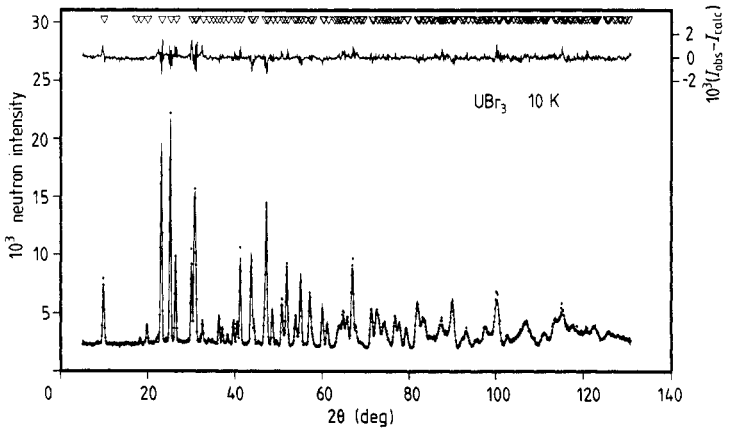

Figure 1. Calculated (———) and observed (·) nuclear neutron diffraction patterns of UBr_3 at 10 K.

Table 1. Structure parameters of UBr_3 and UCl_3 with space group $P6_3/m$ and atom positions 2d for U and 6h for Br, Cl at temperature T. a, c, lattice constants; B, isotropic temperature factor; R_{wp}, R_{In}, agreement values concerning weighted profile and integrated nuclear intensities, respectively. Standard deviations are given within parentheses.

	UBr_3		UCl_3	
	10 K	293 K	10 K	293 K
a (Å)	7.900(2)	7.934(3)	7.412(1)	7.452(6)
c (Å)	4.427(2)	4.438(2)	4.299(2)	4.328(4)
$x_{(Br,Cl)}$	0.2983(2)	0.2992(2)	0.3015(3)	0.3033(5)
$y_{(Br,Cl)}$	0.3846(3)	0.3859(2)	0.3861(3)	0.3883(5)
B_U (Å^2)	0.11(4)	0.78(5)	0.0(1)	0.13(6)
$B_{(Br,Cl)}$ (Å^2)	0.11(2)	0.89(3)	0.15(3)	Not referenced
R_{In} (%)	6.03	6.04	5.17	6.00
R_{wp} (%)	5.41	3.99	5.53	6.14

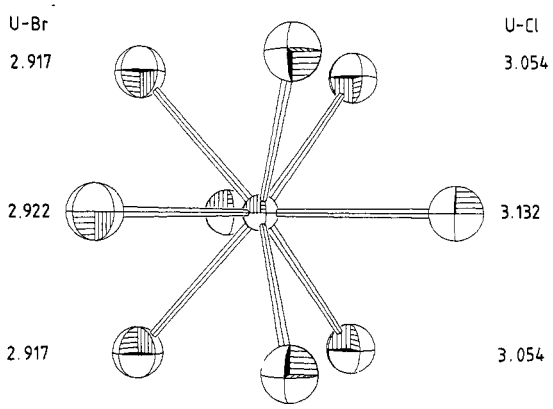

Figure 2. Ninefold coordination of the uranium ions with U–Br and U–Cl distances (Å) for UBr_3 (left) and UCl_3 (right), respectively.

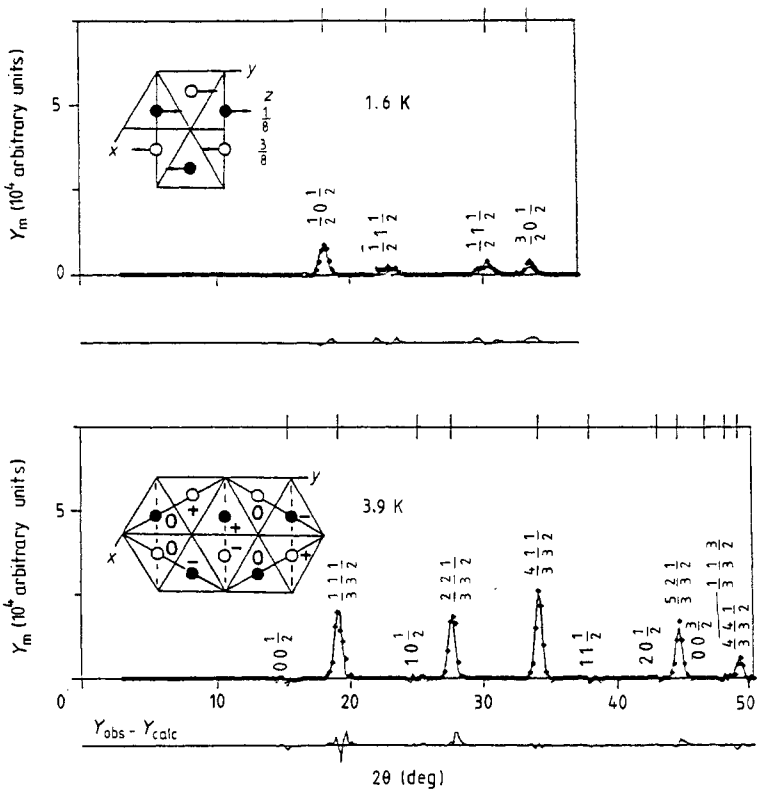

Figure 3. Calculated (——) and observed (·) magnetic neutron diffraction patterns of UBr_3 at 3.9 and 1.6 K. The Miller indices refer to the chemical cell. The insets show projections of the magnetic structures on the basal plane. The complete unit cells are obtained by antitranslation $(0, 0, \frac{1}{2})$. + and − denote the orientations of the magnetic moments parallel and antiparallel to the c axis, respectively. 0 indicates zero value of the average ordered magnetic moment.

the three sublattices. This precludes configurations such as the Potts state ++−. Below 3.0 K in UBr_3 and 3.8 K in UCl_3 we find an orthohexagonal magnetic unit cell with lattice parameters $a_m = \sqrt{3}a$, $b_m = a$, $c_m = 2c$, which is anticentred in the basal plane ($\boldsymbol{q}_1 = [\frac{1}{2}, 0, \frac{1}{2}]$). Magnetic reflections hkl with even l were not observed. Thus the magnetic uranium ions form in all phases antiferromagnetic chains along the c axis, indicating a dominant antiferromagnetic exchange in this direction. In both magnetic configurations the coupling of the two sublattices ($\pm[\frac{2}{3}, \frac{1}{3}, \frac{1}{4}]$ with respect to the chemical cell) cannot be determined from the neutron intensities, i.e. may be ferromagnetic ++ (assumed) or antiferromagnetic +−. The final magnetic structures are included in figure 3, and a summary of the parameters describing the two magnetic phases is given in table 2. The magnetic neutron intensities were refined by means of the standard Rietveld program (Hewat 1979).

At 3.9 K, best agreement between observed and calculated magnetic intensities for UBr_3 and UCl_3 is obtained for a magnetic '0+−' configuration of the three sublattices (one disordered, two antiferromagnetically coupled). The magnetic moments of UBr_3 and UCl_3 of magnitude $\mu_U^{(3.9K)} = 2.08(2)\mu_B$ and $1.8(1)\mu_B$, respectively, are aligned

Table 2. Summary of the magnetic parameters describing UBr_3 and UCl_3.

	UBr_3	UCl_3
T_N (K)	5.38 ± 0.02	6.5 ± 0.05
μ_z (μ_B)	2.08 ± 0.02	1.8 ± 0.1
q_0	$(\frac{1}{3}, \frac{1}{3}, \frac{1}{2})$	
a_m	$a\sqrt{3}$	
c_m	$2c$	
T_t (K)	3.0 ± 0.5	3.8 ± 0.5
μ_x (μ_B)	0.82 ± 0.04	0.8 ± 0.1
q_1	$(\frac{1}{2}, 0, \frac{1}{2})$	
a_m	$a\sqrt{3}$	
b_m	a	
c_m	$2c$	

parallel to the c axis. Agreement values concerning the weighted profile and integrated magnetic neutron intensities are as follows: for UBr_3, $R_{wp} = 19.7\%$ and $R_{Im} = 8.50\%$; for UCl_3, $R_{wp} = 11.6\%$, $R_{Im} = 16.3\%$. Similar arrangements of the moments parallel to the a and b axes or a triangular model in the (x, y) and (y, z) planes yield significantly worse R-factors: $R_{Im} = 53.3\%$, 52.9% and 32.3%, respectively.

At 1.6 K, complete antiferromagnetic order exists, and the magnetic moments of magnitude $\mu_U^{(1.6\,K)} = 0.82(4)\mu_B$ and $0.8(1)\mu_B$ for UBr_3 and UCl_3, respectively, are oriented along the b axis (for UBr_3, $R_{wp} = 33.2\%$ and $R_{Im} = 22.1\%$). The considerably worse agreement in the values is caused by the small magnetic moment. In view of the excessive time needed to collect enough data on UCl_3 to allow us to perform a profile analysis of the magnetic structure at low temperatures, we preferred to measure the temperature dependence of the strongest peaks characteristic for this structure and found complete analogy with the bromide system.

Except for the differences along the c direction and with respect to the number of magnetic sublattices the ground states of UX_3 (X ≡ Br, Cl) resembles $DyGa_2$ (Asmat and Gignoux 1978). With respect to the basal plane this configuration is a possible ground state of the triangular magnetic lattice in two dimensions (Tanaka and Uryu 1976).

The temperature dependence of the magnetic ordering in these systems, which was measured on the two-axis diffractometer, is shown in figure 4. There is a second-order transition at $T_N = 5.4(1)$ K and 6.5(1) K for UBr_3 and UCl_3, respectively. A second magnetic transition occurs at $T_t = 3.0(5)$ K in UBr_3 and 3.8(5) K in UCl_3 with a reorientation of the magnetic moments. No significant hysteresis effects were observed in these transitions. The phase transition at T_t is rather smooth, and there is obviously a coexistence of the 0+− and the orthohexagonal phase over a rather large temperature range.

3. Inelastic neutron scattering analysis of the crystal-field splitting

Inelastic neutron scattering experiments were carried out for polycrystalline samples of UX_3 (X ≡ Br, Cl) with use of a three-axis spectrometer at the reactor Saphir in

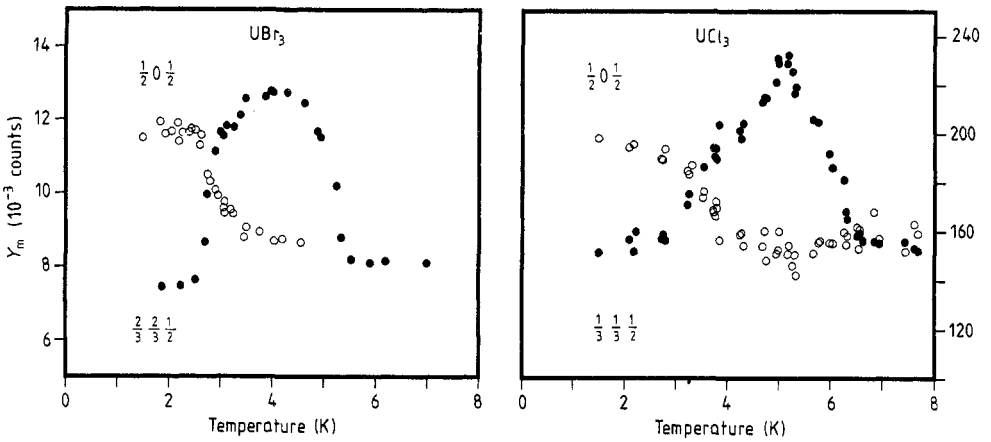

Figure 4. Temperature dependence of the magnetic peak intensities: ●, $0+-$ phase; ○, orthohexagonal phase.

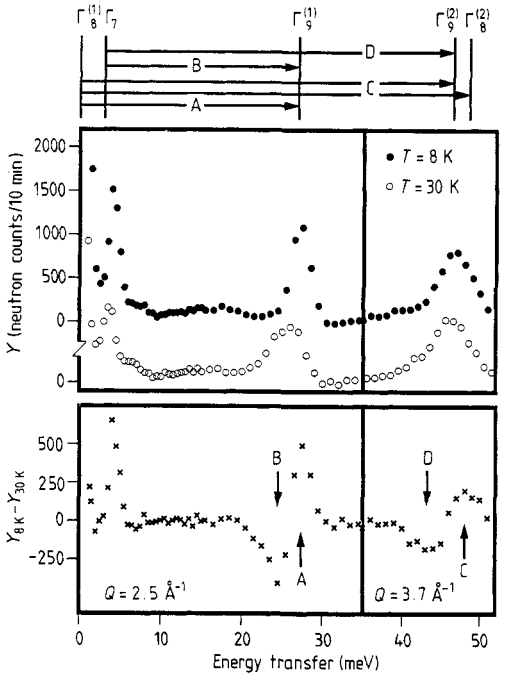

Figure 5. Energy spectra of neutrons scattered from polycrystalline UBr_3. The top of the figure shows the resulting crystal-field level scheme. The arrows denote the allowed and observed crystal-field transitions. The line at 4 meV corresponds to a one-dimensional spin-wave excitation (see text).

Würenlingen. The energy of the scattered neutrons was fixed at 15 meV, and a pyrolytic graphite filter was used to reduce higher-order contamination. Energy spectra were taken at various temperatures and moduli of the scattering vector $\boldsymbol{Q}$ for energy transfers up to 80 meV.

Typical energy spectra obtained for UBr_3 are shown in figure 5. At 8 K there are three well resolved inelastic lines at 4, 27 and 48 meV. Upon increasing the temperature

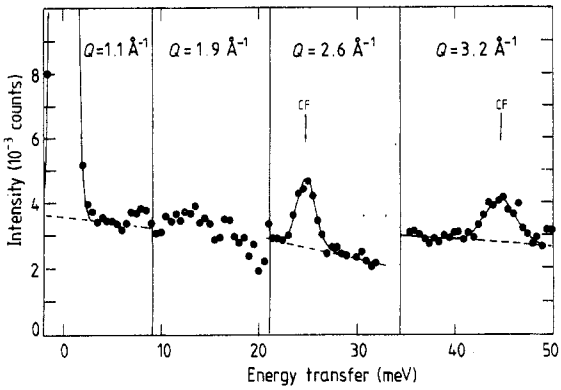

Figure 6. Energy spectra of neutrons scattered from polycrystalline $U_{0.1}La_{0.9}Br_3$ at 8 K. Note the absence of the 4 meV peak. The arrows denote the observed crystal-field transitions.

to 30 K the peak intensities are decreasing, and the lines at 27 and 47 meV are considerably broadened and slightly shifted to lower energies. For $T > 150$ K the intensity of the latter two peaks continues to decrease, whereas the line at 4 meV disappears. The temperature evolution of the peak intensities indicates that the two high-energy lines are crystal-field transitions, whereas the line at 4 meV corresponds to spin-wave excitations within the one-dimensional chains of uranium ions parallel to the c axis. This has been verified by measurements of the magnetically diluted system $U_{0.1}La_{0.9}Br_3$ in which no cooperative phenomena are present. Typical results are shown in figure 6. Indeed the 4 meV excitation is absent, whereas the crystal-field transitions are clearly visible.

The temperature behaviour of the observed energy spectra can be understood by postulating a low-lying first-excited crystal-field state $|\Gamma_n\rangle$ which has a vanishing matrix element $|\langle\Gamma_m|J_\perp|\Gamma_n\rangle|^2$ for the ground-state transition, where $J_\perp$ denotes the component of the total angular momentum operator J perpendicular to the scattering vector $\boldsymbol{Q}$. We arrive at a crystal-field level scheme indicated at the top of figure 5. Our interpretation is supported by considering the difference spectrum shown in the lower part of figure 5. With increasing temperature the ground-state crystal-field transitions (lines A and C) lose intensity, whereas the excited-state transitions (lines B and D) start to show up.

The crystal-field Hamiltonian for a U^{3+} site of C_{3h} symmetry is

$$H_{CEF} = B_2^0 O_2^0 + B_4^0 O_4^0 + B_6^0 O_6^0 + B_6^6 O_6^6, \tag{1}$$

where the B_n^m are crystal-field parameters and the O_n^m are operator equivalents (Stevens 1952). We searched for all possible combinations of the crystal-field parameters to interpret the observed energy spectra and found only one possible parameter set consistent with the experimental data:

$$\begin{aligned} B_2^0 &= (2.5 \pm 0.2) \times 10^{-1} \text{ meV} \\ B_4^0 &= (5 \pm 2) \times 10^{-4} \text{ meV} \\ B_6^0 &= (4.1 \pm 0.2) \times 10^{-4} \text{ meV} \\ |B_6^6| &= (2.7 \pm 0.2) \times 10^{-3} \text{ meV}. \end{aligned} \tag{2}$$

These parameters are different from those derived previously (Murasik and Furrer

Table 3. Observed and calculated CEF levels for UBr_3 (upper part) and UCl_3 (lower part). The eigenfunctions $|\Gamma_n\rangle = \Sigma_{M=-J}^{J} \alpha_{nM}|M\rangle$ and some transition matrix elements $T(\Gamma_n, \Gamma_m) = |\langle\Gamma_m|J_\perp|\Gamma_n\rangle|^2$ are also listed.

Γ_n	E_{obs} (meV)	E_{calc} (meV)	$\|\Gamma_n\rangle$	$T(\Gamma_8^{(1)}, \Gamma_n)$	$T(\Gamma_7, \Gamma_n)$
$\Gamma_8^{(1)}$	0	0	$0.95\|\pm\frac{7}{2}\rangle - 0.30\|\mp\frac{5}{2}\rangle$	15.1	0
Γ_7	3 ± 1	3.2	$\|\pm\frac{1}{2}\rangle$	0	17.0
$\Gamma_9^{(1)}$	27 ± 0.5	26.9	$0.84\|\pm\frac{3}{2}\rangle - 0.55\|\mp\frac{9}{2}\rangle$	5.0	11.2
$\Gamma_9^{(2)}$	46 ± 2	46.8	$0.55\|\pm\frac{3}{2}\rangle + 0.84\|\mp\frac{9}{2}\rangle$	1.8	4.8
$\Gamma_8^{(2)}$	48 ± 1	47.7	$0.95\|\pm\frac{5}{2}\rangle + 0.30\|\mp\frac{7}{2}\rangle$	11.9	0
$\Gamma_8^{(1)}$	0	0	$0.96\|\pm 7\rangle - 0.28\|\mp\frac{5}{2}\rangle$	15.3	0
Γ_7	4 ± 1	4.2	$\|\pm\frac{1}{2}\rangle$	0	17.0
$\Gamma_9^{(1)}$	34 ± 0.5	34.0	$0.83\|\pm\frac{3}{2}\rangle - 0.56\|\mp\frac{9}{2}\rangle$	4.8	11.0
$\Gamma_9^{(2)}$	55 ± 2	55.6	$0.83\|\pm\frac{9}{2}\rangle + 0.56\|\mp\frac{3}{2}\rangle$	1.9	5.0
$\Gamma_8^{(2)}$	58 ± 1	57.7	$0.96\|\pm\frac{5}{2}\rangle + 0.28\|\mp\frac{7}{2}\rangle$	11.0	0

1980), where the line at 4 meV has been falsely attributed to a crystal-field, CEF, transition. The calculated CEF-level scheme as listed in table 3 is in excellent agreement with the observations. Table 3 also lists the matrix elements of selected crystal-field transitions which are in good agreement with the observed intensities.

For UCl_3, energy spectra similar to those for UBr_3 have been observed. Some preliminary data have been presented previously (Murasik *et al* 1985). Owing to the large incoherent scattering cross section of Cl, the observed energy spectra exhibit considerable phonon scattering which partly contaminated the crystal-field transitions (figure 7). In particular, an intense phonon peak with a large high-energy shoulder shows up at 20 meV. At 8 K there are inelastic lines of magnetic origin at 5, 34 and 57 meV. The temperature evolution of these peaks is similar to that for UBr_3. Again the 5 meV line arises from one-dimensional spin-wave excitations (Murasik *et al* 1985), whereas the lines at 34 and 57 meV correspond to crystal-field transitions. The resulting crystal-field level scheme is indicated at the top of figure 7 which may easily be derived by considering the difference spectrum shown in the lower part of figure 7. For UCl_3 we derive the following crystal-field parameters:

$$\begin{aligned} B_2^0 &= (2.8 \pm 0.2) \times 10^{-1}\ \text{meV} \\ B_4^0 &= (6 \pm 2) \times 10^{-4}\ \text{meV} \\ B_6^0 &= (5.1 \pm 0.2) \times 10^{-4}\ \text{meV} \\ |B_6^6| &= (3.0 \pm 0.2) \times 10^{-3}\ \text{meV}. \end{aligned} \tag{3}$$

Table 3 demonstrates the excellent agreement between the observed and calculated energies and intensities of the crystal-field transitions.

4. Discussion

The crystal-field parameters determined in the present work may now be used to calculate the magnetic properties of UBr_3 and UCl_3. The magnetic single-ion susceptibility $\chi_0^{\alpha\alpha}$ ($\alpha = x, y, z$) turns out to be extremely anisotropic with $\chi_0^{xx} = \chi_0^{yy} \ll \chi_0^{zz}$,

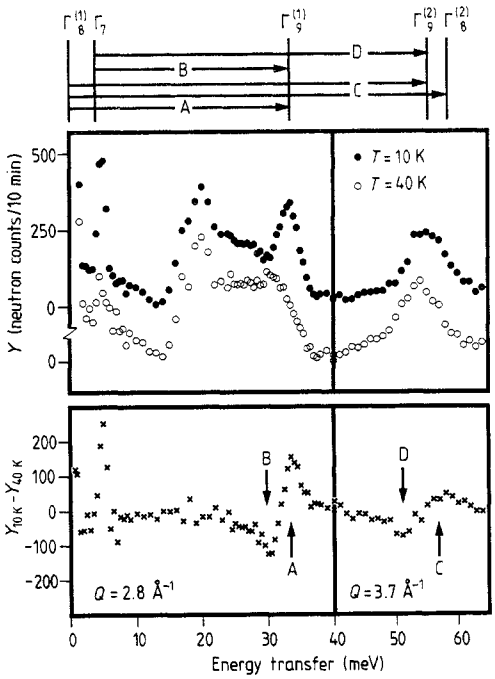

Figure 7. Energy spectra of neutrons scattered from polycrystalline UCl_3. The top of the figure shows the resulting crystal-field level scheme. The arrows denote the allowed and observed crystal-field transitions. The line at 5 meV corresponds to a one-dimensional spin-wave excitation (see text).

yielding the c axis as the easy axis of magnetisation. Indeed, our neutron diffraction experiments gave evidence for three-dimensional antiferromagnetic ordering below T_N with the magnetic moments aligned along the c axis. The question then arises of which mechanism is responsible for the magnetic phase transition at T_t into an antiferromagnetic structure with the moments oriented parallel to the b axis.

We have performed a mean-field calculation and compared the free energies in the two magnetic phases. A similar investigation for UBr_3 has recently been performed by Lyzwa and Erdös (1987). For the μ_x phase with $\boldsymbol{\mu} \| \boldsymbol{b}$ the free energy is given by

$$F_x = -k_B T \ln Z - J^{xx}(\boldsymbol{q}_1)\langle S^x \rangle^2 \tag{4}$$

and for the μ_z phase with $\boldsymbol{\mu} \| \boldsymbol{c}$ we have

$$F_z = \tfrac{2}{3}[-k_B T \ln Z - J^{zz}(\boldsymbol{q}_0)\langle S^z \rangle^2] - \tfrac{1}{3} k_B T \ln Z_p \tag{5}$$

where Z and Z_p are the partition functions in the antiferromagnetic and paramagnetic phases, respectively, and $J^{xx}(\boldsymbol{q}_1)$ and $J^{zz}(\boldsymbol{q}_0)$ are the Fourier-transformed exchange functions in the μ_x and μ_z phases with ordering wavevectors $\boldsymbol{q}_1$ and $\boldsymbol{q}_0$, respectively. $J^{zz}(\boldsymbol{q}_0)$ was adjusted to predict the observed Néel temperature correctly, and $J^{xx}(\boldsymbol{q}_1)$ was determined by equalising the free energies F_x and F_z at the transition temperature T_t. The value of the exchange functions are listed in table 2. The results of the calculations are shown in figure 8 and are in reasonable agreement with the observations. In particular, the drastic reduction in the ordered moment below the free-ion value is excellently reproduced for the μ_x phase. On the other hand, the initial slope of the zero-field magnetisation below T_N considerably deviates from the theoretical curve; however, a mean-field calculation is known to be a poor approximation close to T_N.

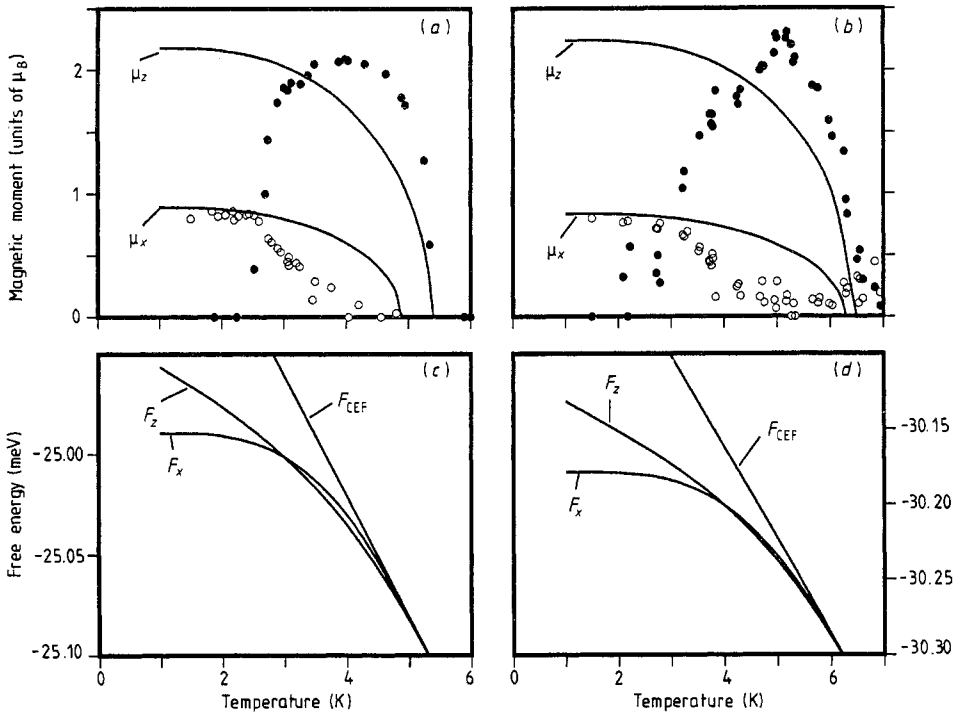

Figure 8. Comparison between our calculations and the experiment for (*a*), (*c*) UBr_3 and (*b*), (*d*) UCl_3: (*a*), (*b*) magnetic moment (●, $\frac{2}{3}\frac{2}{3}\frac{1}{2}$; ○, $\frac{1}{2}0\frac{1}{2}$; ———, calculation); (*c*), (*d*) free energy of the different phases, where F_{CEF} denotes the paramagnetic contribution.

Table 4. Coordination factors for UBr_3 and UCl_3.

	UBr_3	UCl_3
γ_2^0 (Å^{-3})	0.595 08	0.792 08
γ_4^0 (Å^{-5})	0.062 84	0.065 84
γ_6^0 (Å^{-7})	0.005 09	0.008 28
γ_6^6 (Å^{-7})	0.044 82	0.068 78
A_2^0 (meV Å^3)	4.2 ± 0.3	3.5 ± 0.3
A_4^0 (meV Å^5)	80 ± 32	91 ± 30
A_6^0 (meV Å^7)	805 ± 39	616 ± 24
A_6^6 (meV Å^7)	60.2 ± 4.5	43.6 ± 2.9

A relatively simple understanding of the crystal-field parameters may result from a calculation which takes account of the neighbouring coordination polyhedra around the U^{3+} ions. The crystal-field parameters are then given by

$$B_n^m = A_n^m \gamma_n^m. \tag{6}$$

The coordination factors γ_n^m as defined, for example, by Hutchings (1964) are listed in table 4 for the nearest-neighbour Br and Cl polyhedra. We find that the reduced crystal-field parameters A_n^m obtained for UCl_3 are systematically smaller by about 20% than

the corresponding values evaluated for UBr_3. This means that the crystal-field parameters of UX_3 are strongly correlated by geometrical coordination, i.e. the structural correlation is quantitatively established up to an overall scaling factor for the crystal-field potential. A similar behaviour of the crystal-field parameters has already been reported for the isostructural compounds PrX_3 (Schmid *et al* 1987).

Finally we discuss the observation of the strong inelastic lines at 4 meV and 5 meV in UBr_3 and UCl_3, respectively, which have been attributed to one-dimensional spin-wave excitations along the c axis. The spin-wave dispersion of a one-dimensional magnet is given by (Achiwa 1969)

$$h\omega(q_c) = 4|J|S[(1 + |D/8J|)^2 - (\cos q_c)^2]^{1/2} \tag{7}$$

where the anisotropy parameter D determines the spin-wave energy gap at $q_c = 0$. Our inelastic neutron scattering experiments on polycrystalline material essentially sample the zone-boundary spin waves with $q_c = \pi$. For $D = 0$, $J = J^{xx}(\boldsymbol{q}_1)$ and $S = \frac{7}{2}g_J$ (consistent with the $\Gamma_8^{(1)}$ ground state; see table 3); we find that $h\omega(q_c = \pi) = 3.4$ meV and 4.5 meV for UBr_3 and UCl_3, respectively. These zone-boundary spin-wave energies are very close to the observed spin-wave excitations at 4 meV and 5 meV, which means that the spin-wave energy gap is less than 1 meV.

5. Conclusions

The 5f compounds UX_3 show remarkable magnetic phase transitions, which are caused by crystal-field effects and anisotropic magnetic interactions. To our knowledge, UBr_3 and UCl_3 are the first 5f-electron systems which show features of one-dimensional magnetism at higher temperatures. These phenomena should be studied by neutron scattering in more detail on single crystals. Such investigations could prove the anticipated one-dimensional magnetic ordering as well as provide the parameters of the magnetic interactions from the dispersion of the magnetic excitations.

Acknowledgments

Discussions with B Hälg are gratefully acknowledged. This research was partly supported by the Swiss National Science Foundation.

Note added in proof. A recent study byPlumer and Caillé (1989) based on a Landau-type free energy functional of the spin density suggests that for UBr_3 (and most likely also for UCl_3) an intermediate phase characterised by the superposition of the μ_z phase with $\boldsymbol{\mu} \| \boldsymbol{c}$ and the μ_x phase with $\boldsymbol{\mu} \| \boldsymbol{b}$ can indeed be stabilised, which confirms our observation of the coexistence of the two phases at around T_t.

References

Achiwa N 1969 *J. Phys. Soc. Japan* **27** 561
Asmat H and Gignoux D 1978 *Rare Earths and Actinides 1977* (*Inst. Phys. Conf. Ser. 37*) ed W D Corner and B K Tanner (Bristol: Institute of Physics) p 286
Berger M and Sienko M J 1968 *Inorg. Chem.* **6** 324
Brown D 1968 *Halides of the Lanthanides and Actinides* (London: Wiley) p 83
Hewat A W 1979 *UKAEA Harwell Report* R7350

Hutchings M T 1964 *Solid State Physics* vol 16, ed F Seitz and D Turnbull (New York: Academic) p 227
Jones E R Jr, Hendricks M E, Stone J A and Karraker D G 1974 *J. Chem. Phys.* **60** 2088
Levy J H, Taylor J C and Wilson P W 1975a *Acta Crystallogr.* B **31** 880
—— 1975b *J. Less-Common Met.* **39** 265
Lyzwa R and Erdös P 1987 *Phys. Rev.* B **36** 1587
Murasik A, Fischer P, Furrer A, Schmid B and Szczepaniak W 1986 *J. Less-Common Met.* **121** 151
Murasik A, Fischer P, Furrer A and Szczepaniak W 1985 *J. Phys. C: Solid State Phys.* **18** 2909
Murasik A, Fischer P and Szczepaniak W 1981 *J. Phys. C: Solid State Phys.* **14** 1847
Murasik A and Furrer A 1980 *Physica* B **102** 185
Plumer and Caillé 1989 *Phys. Rev.* B **40** 196
Schmid B, Hälg B, Furrer A, Urland W and Kremer R 1987 *J. Appl. Phys.* **61** 3426
Stevens K W H 1952 *Proc. Phys. Soc.* A **65** 209
Tanaka Y and Uryu N 1976 *Prog. Theor. Phys.* **55** 1356
Taylor J C and Wilson P W 1974 *Acta Crystallogr.* B **30** 2803
Wiles D B and Young R A 1981 *J. Appl. Crystallogr.* **14** 149